Two-dimensional optical phased array antenna on silicon-on-insulator

Karel Van Acoleyen,[1,*] **Hendrik Rogier,**[2] **and Roel Baets**[1]

[1]*Department of Information Technology (INTEC) - Photonics Research Group,*
Ghent University - imec, Sint-Pietersnieuwstraat 41, B-9000 Ghent, Belgium
[2]*Department of Information Technology (INTEC) - Electromagnetics Group,*
Ghent University, Sint-Pietersnieuwstraat 41, B-9000 Ghent, Belgium

*karel.vanacoleyen@intec.ugent.be

Abstract: Optical wireless links can offer a very large bandwidth and can act as a complementary technology to radio-frequency links. However, optical components nowadays are rather bulky. Therefore, we have investigated the potential of silicon photonics to fabricate integrated components for wireless optical communication. This paper presents a two-dimensional phased array antenna consisting of grating couplers that couple light off-chip. Wavelength steering of $0.24°$/nm is presented, reducing the need of active phase modulators. The required steering range is $1.5°$. The 3dB angular coverage range of these antennas is 0.007π sr with a directivity of more than 38dBi and antenna losses smaller than 3dB.

© 2010 Optical Society of America

OCIS codes: (050.1950) Diffraction gratings; (060.2605) Free-space optical communication; (130.3120) Integrated optics devices.

References and links

1. J. M. Kahn and J. R. Barry, "Wireless infrared communications," Proc. IEEE **85**, 265–298 (1997).
2. K. Van Acoleyen, W. Bogaerts, J. Jágerská, N. Le Thomas, R. Houdré, and R. Baets, "Off-chip beam steering with a one-dimensional optical phased array on silicon-on-insulator," Opt. Lett. **34**, 1477–1479 (2009).
3. P. F. McManamon, T. A. Dorschner, D. L. Corkum, L. J. Friedman, D. S. Hobbs, M. Holz, S. Liberman, H. Q. Nguyen, D. P. Resler, R. C. Sharp, and E. A. Watson, "Optical phased array technology," Proc. IEEE **84**, 268–298 (1996).
4. R. J. Green, H. Joshi, M. D. Higgins, and M. S. Leeson, "Recent developments in indoor optical wireless systems," IET Commun. Mag. **2**, 3–10 (2008).
5. S. K. Selvaraja, P. Jaenen, W. Bogaerts, D. Van Thourhout, P. Dumon, and R. Baets, "Fabrication of Photonic Wire and Crystal Circuits in Silicon-on-Insulator Using 193-nm Optical Lithography," J. Lightwave Technol. **27**, 4076–4083 (2009).
6. ePIXfab, "The silicon photonics platform," http://www.epixfab.eu/.
7. G. Roelkens, D. Vermeulen, D. Van Thourhout, R. Baets, S. Brision, P. Lyan, P. Gautier, and J. M. Fedeli, "High efficiency diffractive grating couplers for interfacing a single mode optical fiber with a nanophotonic silicon-on-insulator waveguide circuit," Appl. Phys. Lett. **92**, 131101 (2008).
8. F. Van Laere, T. Claes, J. Schrauwen, S. Scheerlinck, W. Bogaerts, D. Taillaert, L. O'Faolain, D. Van Thourhout, and R. Baets, "Compact focusing grating couplers for silicon-on-insulator integrated circuits," IEEE Photon. Technol. Lett. **19**, 1919–1921 (2007).
9. N. Le Thomas, R. Houdré, M. V. Kotlyar, D. O'Brien, and T. E. Krauss, "Exploring light propagating in photonic crystals with Fourier optics," J. Opt. Soc. Am. B **24**, 2964–2971 (2007).
10. D. Vermeulen, S. Selvaraja, G. Verheyen, P. Lepage, W. Bogaerts, and G. Roelkens, "High-efficiency Silicon-On-Insulator Fiber-to-Chip Grating Couplers Using a Silicon Overlay," in "Group IV Photonics," (United States, 2009), p. FPd1.
11. K. Van Acoleyen, H. Rogier, and R. Baets, "Feasibility of Integrated Optical Phased Arrays for Indoor Wireless Optical Links," in "Optical Communication, 2009. ECOC '09. 35th European Conference on," (Vienna, Austria, 2009), p. P4.18.

---

1. Introduction

On the one hands, as the available radio spectrum is getting more and more congested, people are looking for solutions by either using a different carrier frequency (60GHz band), MIMO (Multiple-Input-Multiple-Output) communication or by applying UWB (UltraWide Band). The optical domain, on the other hand, has a virtually unlimited bandwidth available free from regulations. Optical systems do not suffer from electromagnetic interference, provide an increased security and could serve either as a stand-alone technology or in hybrid optical-RF systems. Therefore, these systems are getting increased attention for indoor wireless links [1].

As the present wireless optical systems consist of bulky components, we have investigated the use of an integrated technology to fabricate components for wireless optical links. For that purpose, we have made use of the CMOS (Complementary Metal-Oxide Semiconductor) compatible silicon-on-insulator (SOI) platform allowing dense integration. Beam scanning is important for directive links and can be done by wavelength scanning or active phase tuning. Whereas for an $N \times N$ array, N^2 phase tuners are needed to perform full two-dimensional beam scanning, this number can be reduced to N by using wavelength scanning in one direction.

This paper presents a two-dimensional optical phased array (OPA) fabricated on SOI. OPAs allow very stable, rapid and precise beam steering without mechanical motion, making them robust and insensitive to external constraints such as acceleration [2,3]. When choosing a large element spacing, we will obtain multiple higher-order grating lobes in the far-field. This usually unwanted effect can find applications in multipath optical links [4]. The beam direction is controlled by tuning the phase relationship between an array of transmitters. This is performed by wavelength tuning in one direction thanks to delay lines between the elements. Integration with N active phase tuners would result in full two-dimensional steering of an $N \times N$ array. Furthermore, these OPAs could be used in coherent receiver schemes.

Section 2 describes the design and fabrication of the component using the SOI platform. Section 3 discusses the Fourier imaging measurement setup to investigate the far-field properties of the component. Section 4 provides the measurement results and section 5 presents a conclusion.

2. Design and Fabrication

The component shown in Fig. 1 was fabricated on SOI with an oxide thickness of 2μm and a silicon top layer thickness of 220nm using standard CMOS processes in *imec*. This high index contrast platform allows a high level of integration with small, low-loss waveguides with bend radii down to 5μm~ []Selvaraja2009, ePIXfab. Two etching steps are used, one of 220nm for etching the waveguides and the multimode interference (MMI) splitters and the second of 70nm to etch the grating couplers. The input waveguide in Fig. 1 is connected to a grating coupler to couple light into the waveguide system. Such a grating coupler uses the principle of diffraction to couple light from a single mode optical fiber into the TE-like mode of a 10μm waveguide [7]. The waveguide then tapers down to a 450nm wide photonic wire being the input waveguide in Fig. 1. This waveguide is then split by a MMI tree into K output waveguides, with K being 4 for a 2 by 2 array and 16 for a 4 by 4 array. The radiating elements consist of a focusing grating coupler that couples out light in a near vertical direction [8].

3. Measurement Setup

Figure 2 schematically shows the Fourier-space imaging technique that was used to investigate the off-chip radiation pattern [9]. The far-field of the component is imaged on the back-focal plane of a microscope objective with numerical aperture NA=0.5. In this plane, one point corresponds to a unique direction of off-chip emission and can be parameterized by $(\sin\theta, \sin\phi)$. This back-focal plane is then brought back to a CCD camera by means of two lenses. The pa-
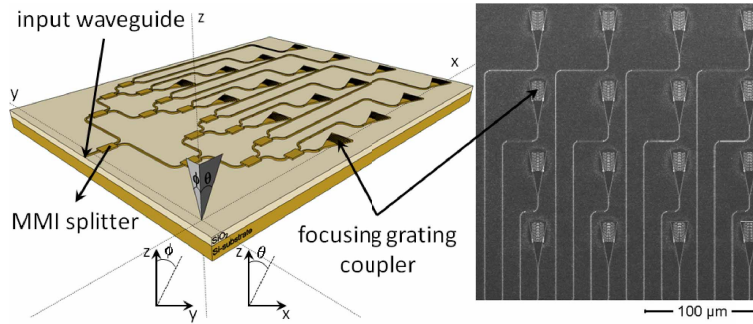
Fig. 1. Two-dimensional OPA on SOI: schematic view (left), top-view SEM picture of the measured 4×4 OPA (right). Light coming from the input waveguide is split via a MMI tree and then coupled out-of-plane using focusing grating couplers.

rameters θ and ϕ are defined as the out-coupling angles in the longitudinal plane and transverse plane (i.e. perpendicular to the waveguide axis) with respect to the normal of the sample surface (Fig. 1).
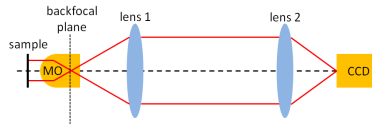

Fig. 2. Schematic view of the Fourier imaging setup: the backfocal plane of the microscope objective (MO) is brought back to the CCD camera by means of two lenses.

4. Measurement Results and Discussion

4.1. Far-field pattern

Figure 3(a) presents a schematic view of the cross section of a focusing grating coupler. The far-field of this focusing grating coupler is shown in Fig. 3(b). This far-field determines the steering range of the OPA. The envelope will shift in the θ-direction when changing the wavelength due to the grating equation

$$\sin \theta = \frac{\Lambda n_{eff,gc} - \lambda_0}{n_{ct} \Lambda},\tag{1}$$

with $\Lambda = 625$nm being the period of the grating, λ_0 the free-space wavelength, $n_{eff,gc}$ the effective index of the guided mode of the coupler region (≈ 2.67 at $\lambda_0 = 1550$nm) and n_{ct} the refractive index of the background, which is air in this case. The shift in θ angle as well as the change in beam width can be found in Fig. 3(c). The latter does not change significantly.

These grating couplers are placed in a $N \times M$ array configuration with positions $\mathbf{s}_{mn} = m\Lambda_x \mathbf{u}_x + n\Lambda_y \mathbf{u}_y$ with Λ_x and Λ_y the spacing of the elements in the x- and y-direction, respectively, and where $m = 0 \dots M - 1$ and $n = 0 \dots N - 1$. The far-field is calculated by multiplication of the far-field of one grating coupler with the array factor $T(\theta, \phi)$:

$$T(\theta, \phi) = \sum_{m=0}^{M-1} \sum_{n=0}^{N-1} A_{mn} e^{-j\beta_{mn}} e^{j\mathbf{k} \cdot \mathbf{s}_{mn}} = \sum_{m=0}^{M-1} \sum_{n=0}^{N-1} A_{mn} e^{-j\beta_{mn}} e^{jk_0[m\Lambda_x \sin \theta + n\Lambda_y \sin \phi]},\tag{2}$$

where β_{mn} is the phase delay between the elements, $\mathbf{k}$ is the wave vector (in air) with magnitude k_0 and A_{mn} is the amplitude of each element which is constant in our case and further assumed
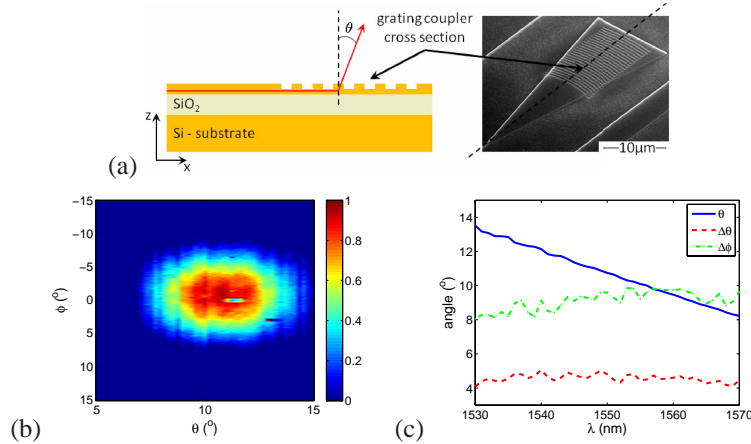
Fig. 3. (a) Schematic view of a cross section of a grating coupler. (b) Far-field pattern of the focusing grating coupler at a wavelength of 1550nm. The FWHM width in the θ-direction is 4.8° and in the ϕ-direction is 9.6°. (c) Out-coupling angle θ (blue), FWHM θ (red) and FWHM ϕ (green) as a function of wavelength.

to be 1. Having only a length difference ΔL between the elements in the x-direction, we obtain:

$$\beta_{mn} = n_{eff}\frac{2\pi}{\lambda}\Delta L_{mn} = mn_{eff}\frac{2\pi}{\lambda}\Delta L, \tag{3}$$

with n_{eff} the effective index of the fundamental TE-like mode. The array factor is calculated in closed form:

$$T(\theta,\phi) = e^{j\left[(k_0\Lambda_x\sin\theta - k_0n_{eff}\Delta L)\frac{M-1}{2} + (k_0\Lambda_y\sin\phi)\frac{N-1}{2}\right]} \frac{\sin\left(M\frac{k_0\Lambda_x\sin\theta - k_0n_{eff}\Delta L}{2}\right)}{\sin\left(\frac{k_0\Lambda_x\sin\theta - k_0n_{eff}\Delta L}{2}\right)} \frac{\sin\left(N\frac{k_0\Lambda_y\sin\phi}{2}\right)}{\sin\left(\frac{k_0\Lambda_y\sin\phi}{2}\right)}. \tag{4}$$

The array factor exhibits a maximum in the θ-direction for

$$\sin\theta = q\frac{\lambda}{\Lambda_x} + \frac{n_{eff}\Delta L}{\Lambda_x}, \tag{5}$$

for integer q. Due to the delay lines, the absolute value of q will be large. The beams will shift at a rate of

$$\frac{d\theta}{d\lambda} \approx \frac{d\sin\theta}{d\lambda} = \frac{q}{\Lambda_x} + \frac{dn_{eff}}{d\lambda}\frac{\Delta L}{\Lambda_x}, \tag{6}$$

where the angle θ is assumed to be relatively small. Note that q is negative so that the beam will shift in the negative θ-direction for increasing wavelength. The effect of dispersion cannot be neglected in this high index contrast platform. There are two main contributions to dispersion: material dispersion and waveguide dispersion. Whereas the former is relatively weak for the small wavelength range considered in this paper, the latter has a significant influence due to the extremely high confinement in the small photonic wires. The change of n_{eff} as a function of wavelength is negative as well, being about -0.013/nm around $\lambda = 1.55\mu$m.

Figure 4 shows the measured far-field pattern of a 2×2 OPA together with the theoretical far-field. Figure 5 shows a cross section of the far-field along the θ-direction for a 2×2 and 4×4 OPA. The asymmetry of these patterns is due to the delay lines. The parameters of these OPAs are found in Table 1. The larger discrepancy for the 4×4 OPA is due to the saturation of
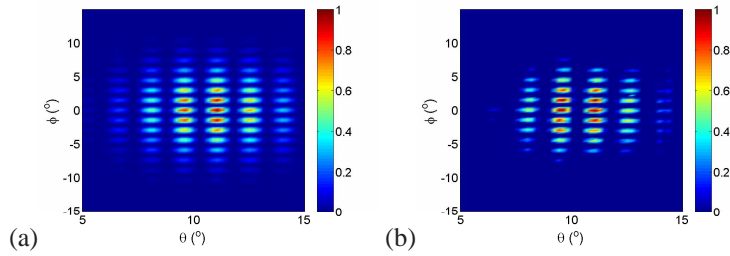
Fig. 4. Theoretical (a) and measured (b) far-field pattern of a 2×2 OPA at a wavelength of 1550nm, the parameters are found in Table 1.

the camera pixels at the higher intensities. When the OPA becomes large, the beams are only a few pixels wide resulting in less accurate measurements with our setup.
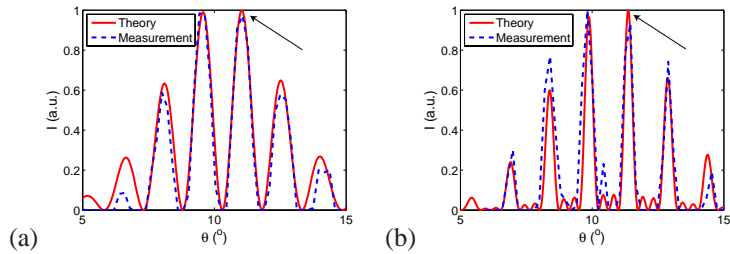

Fig. 5. Cross section at $\phi = 0°$ of the far-field pattern of a (a) 2×2 and (b) 4×4 OPA at a wavelength of 1550nm, the parameters of the OPA are found in Table 1. The indicated peak has a width of (a) $0.66°$ and (b) $0.36°$.

4.2. Steering capability

By changing the wavelength, the envelope of the far-field will shift [Fig. 3(c)], but also the array factor will shift due to the delay lines. Figure 6(a) shows the shift of the peak indicated in Fig. 5 by an arrow. For the 2×2 OPA this shift is about $-0.24°$/nm whereas for the 4×4 OPA it is $-0.20°$/nm. The latter is smaller since the ratio $\Delta L / \Lambda_x$ is smaller. The contribution of dispersion is about $-0.11°$/nm for the 2×2 OPA and $-0.09°$/nm for the 4×4 OPA.
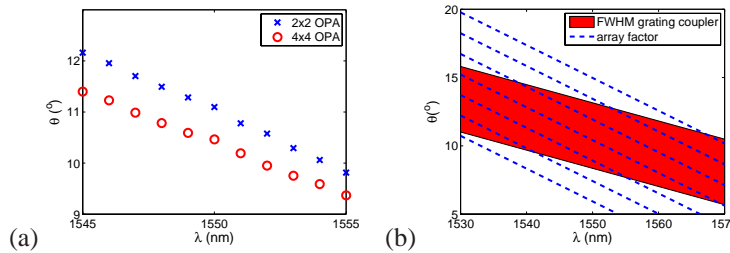

Fig. 6. (a) Shift of the peak shown in Fig. 5 by changing the wavelength. (b) Schematic view of wavelength steering capability. The red region represents the shift of the FWHM of the envelope of our far-field pattern (i.e. the far-field pattern of one grating coupler), while the blue dashed lines represents the shift of the individual emission lobes with wavelength.

Figure 6(b) shows the coverage range as a function of wavelength. Steering could be performed by first steering the envelope while fine tuning is done by steering the array factor. As the envelope shifts, the array factor peaks will shift out of the envelope while new peaks will shift in. Since the peaks are spaced about $\arcsin(\lambda/\Lambda) = 1.48°$ (at 1550nm for a 60µm spacing), the required wavelength shift for fine tuning is not more than 7nm. By making the delay lines longer, this number can be further decreased.

Steering in the ϕ-direction can be performed by incorporating phase tuners. To steer the beam of an $N \times N$ array in the ϕ-direction, N modulators are needed where in principle we only need to define the phase difference between each arm.

4.3. Efficiency

The waveguide losses in the SOI platform were shown to be less than 3dB/cm while the bending loss is 0.013dB/bend. Since the total waveguide length is in the order of mm, this loss is not more than 1dB [5]. The grating couplers fabricated with one etch of 70nm in a 220nm silicon top layer have a mean efficiency of about -5.2dB. The use of a silicon overlay can enhance the efficiency up to -1.6dB [10]. This is the efficiency of the grating coupler when it is used to guide light between an optical fiber and a photonic integrated circuit. The efficiency to free space, instead of to an optical fiber, will be better. The total loss from waveguide input to free space can thus be limited to less than 3dB.

As shown in [11], the directivity of our OPA does not depend on element spacing but only on the effective total radiating aperture. The theoretical and measured directivity, calculated by

$$D(\theta,\phi) = 4\pi \frac{I(\theta,\phi)}{P_{tot}}, \tag{7}$$

with P_{tot} the total power radiated by the OPA, for the peak indicated by an arrow in Fig. 5, is given in Table 1. A good agreement with the theory can be seen. For the 2×2 OPA, the gain is even higher because the lower intensity levels are not measured very accurately.

Table 1. Parameters of the measured OPAs.

$N = M$	$\Lambda_x = \Lambda_y$ (µm)	ΔL (µm)	D_{th} (dBi)	D_{meas} (dBi)
2	60	87.2	34.9	37.0
4	60	72.2	40.0	38.4

5. Conclusion

A two-dimensional OPA on SOI has been presented. Steering in one direction has been shown by means of wavelength tuning. Thanks to delay lines between the elements and the dispersion of these delay lines, a steering speed of 0.24°/nm is presented. This speed is easily increased by increasing the delay line length between the elements. The lobes of the OPA are spaced 1.5° apart and the 3dB coverage range is about 10° in both directions ($\approx 0.007\pi$ sr), with a directivity of more than 38dBi while the antenna losses are smaller than 3dB. Complete two-dimensional steering can be performed by adding phase tuners on the waveguides. In this way, full two-dimensional beam steering is possible with limited need of active phase tuning.